

A Comparative Corrosion Study on Traditional and Melt-Spinning 7075 Al Alloy



Sieglind Ngai, Tungwai Ngai, Yongliang Ou, Weipeng Zhang and Liejun Li

Abstract Rapidly solidified 7075 Al alloy ribbons were prepared by melt-spinning. Sintered 7075 compacts with fine-grain microstructure were obtained by spark plasma sintering of the chopped melt-spun ribbons at different sintering temperatures. The corrosion behavior of the sintered 7075 alloy was examined and compared to that of the 7075-T6 bulk by electrochemical and immersion experiments carried out in NaCl solution. Microstructures of the consolidated samples before and after corrosion tests were examined by optical microscope and scanning electron microscope. Ratios of corrosion after immersion tests were measured by an image analyzing software. Results of this study suggest that the sintered material exhibited slightly poorer corrosion resistance than the bulk 7075 alloy and the porosity adversely affect the corrosion behaviors of the sintered material.

Keywords Fine-grain 7075 Al alloy · Powder metallurgy · Melt-spinning Corrosion behavior · Electrochemical test

Introduction

Rapid solidification (RS) with cooling rate of 10^4 – 10^6 Ks⁻¹ can produce alloys with unconventional characteristic such as extended solute solubility, less segregation, better homogeneity, much finer grain size and in some cases, even the formation of nano-crystalline and amorphous phases [1]. Melt spinning is among the most commonly used methods that can significantly modify the alloy

S. Ngai (✉) · T. Ngai · Y. Ou · W. Zhang · L. Li
National Engineering Research Center of Near-Net-Shape Forming Technology for Metallic Materials, South China University of Technology, Guangzhou 510640, People's Republic of China
e-mail: mikitoози@gmail.com

T. Ngai
e-mail: dhni@scut.edu.cn

microstructure [2]. Recent researches on the rapidly solidified Al alloys are mostly concentrated on Al–Si–X alloys, which are aimed at automotive applications such as connecting rod, cylinder sleeve, piston and valve retainer etc. [3–5]. Heat-treatable aluminum alloys are extensively used in various industries because of their low density and general acceptable mechanical properties. The outstanding high strength 7075 aluminum alloy (Al–Zn–Mg–Cu) has been widely used in aerospace industry [6]. The remarkable mechanical properties of the 7075 alloy are mainly attributed to the nano sized precipitation and sub-micron sized dispersoids formed from those alloying elements. The presence of these precipitations and intermetallic phases complicates the electrochemical behaviors of the alloy. Other than the basic alloying elements, appreciable amounts of minor constituents or impurity elements such as Si, Ti etc. may intensify the corrosion susceptibility of the alloy. Corrosion involving Al alloys has long been a perplexing problem in aviation industry [7]. For instance, pitting degrades the fatigue properties of 7075 alloy significantly [8, 9]. The presence of corrosion pits shortened the fatigue crack initiation life by a factor of two to three and decreases the fatigue crack initiation threshold by about 50% [9]. Few studies concerning the rapid solidification of 7075 alloy were performed [10–12]. For instance, Rokni et al. investigated the microstructural evolution of gas atomized 7075 Al powder during high-pressure cold sprayed deposition. However, no corrosion experiment was performed [10]. They obtained high quality coatings with limited porosity. The severely deformed particle/particle boundaries lead to the formation of an ultrafine-grain structure and a low density of large angle grain boundaries. While, for small grains precipitates were distributed primarily at grain boundaries. In a recent study conducted by Qu and his co-workers, they found discrete, but chain-like grain boundary precipitates together with some dispersively distributed nano-sized matrix precipitates in a sprayed formed and T6 heat-treated 7075 alloy (with a grain size about 30 μm) [11]. The presence of continuous Mg and Zn containing precipitations at grain boundary has significant effect on the corrosion behaviors of the alloy. But they did not perform any corrosion study. Up to now, limited work has been done on the electrochemical characterization of melt-spun 7075 Al alloy.

In this study, 7075 ribbons were obtained by melt-spinning. The ribbons were then sintered into compacts by spark plasma sintering. Corrosion behavior of the 7075-T6 bulk and sintered materials were studied and compared by using electrochemical and immersion corrosion tests.

Experimental

Melt-spinning 7075 ribbons were produced under vacuum (2.0×10^{-3} Pa) by using a WK-II melt-spinning machine (Physcience Opto-electronics Co., Ltd., Beijing), having a copper wheel with a diameter of 230 mm rotating at 2500 r.p.m. By employing a crucible gas pressure of 250 mbar, a crucible nozzle of ~ 1.0 mm,

a distance between nozzle and wheel of 2.25 mm and an angle between crucible and off-centre line of 3° , ribbons of $\sim 40 \mu\text{m}$ thick, 1.8–2.0 mm wide and 70–1000 mm in length were obtained. The temperature of the melt before ejection was 750°C (about 100°C above the liquidus).

Spark Plasma Sintering The rapidly solidified ribbons were cut into small chips of about $2 \text{ mm} \times 3 \text{ mm} \times 0.1 \text{ mm}$ in size. About 6 g of this chips was placed into a 20 mm diameter graphite mold and sintered at 450, 500 and 520°C under vacuum ($1 \times 10^{-3} \text{ Pa}$) by using a Dr. Sinter Type SPS-825 spark plasma sintering apparatus (Sumitomo Coal Co. Ltd, Japan). The heating rate and soaking time were $50^\circ\text{C}/\text{min}$ and 15 min, respectively. An uniaxial pressures was maintained constant at 30 MPa during sintering. Density of the samples was measured by using Archimedes method.

Electrochemical Tests Only samples sintered at 500°C were being used in electrochemical tests and immersion tests. Before each single experiment, samples were ground by a wet 2000 grit SiC paper. All electrochemical experiments were carried out in 0.1 M NaCl solution (450 mL) using a standard three-electrode cell (PAR), involving a saturated calomel electrode (SCE) and a graphite counter electrode. Electrochemical corrosion potential (E_{corr}) was collected by a potentiostat (IVIUM VERTEX). Potentiodynamic polarization scans (PD) were conducted with a starting potential 300 mV below the open circuit potential (OCP) under a scan rate of 0.2 mVs^{-1} . The open circuit potential was measured from an open circuit setup (OC) after a holding time of 8ks. Values of corrosion current density (I_{corr}) were determined from Tafel plots of the polarization data. The experiments were carried out in air under a constant temperature of 25°C . The reported values are averages from three individual measurements.

Immersion Tests All samples were ground to a 2000 grit finish before immersion tests. After 7 days of immersion in 0.1 and 0.6 M NaCl solution, corrosion products were removed by cleaning the samples in 7% HNO_3 under ultra-sound. Microstructure of these samples was examined by an optical microscope (Leica DMI 5000 M) before and after immersion tests. Scanning electron microscopy (Zeiss Merlin) was employed to perform microstructural characterization. Ratios of corrosion characteristics after immersion tests were measured by an image analyzing software (Image J), using a grey scale threshold based image segmentation method. Each reported ratio is an average of 11 measurements.

Material Characterization Microstructure of the samples was characterized using optical and scanning electron microscopy. All samples were prepared by standard metallographic techniques. The ribbon was mounted in epoxy resin at room temperature prior to grinding and polishing. Sample hardness was measured by using a load of 100 g, and each reported hardness value is an average of 10 different tests.

Results and Discussion

Figure 1 is SEM micrographs showing dendritic structure on the free-side of the melt-spun 7075 ribbon. Due to the rapid cooling caused by the fast spinning Cu wheel, the wheel-side (chill side) of the ribbon is a thin featureless zone and it connected to the free-side with a transition zone consist of columnar grain structure. Due to the outgrowth of columnar grains, the free-surface of the ribbon is not perfectly smooth, as shown in Fig. 1a, tiny bumps and ridges can be seen. The large round shaped grains (about 2–3 μm in diameter with very weak dendritic growth on the rim) found in Fig. 1b are evidence of the outgrowth of columnar grains from the chill side of the ribbon, while, the rest are mostly dendrites with dendritic arm spacing less than a micron.

Figure 2a shows typical microstructure of the 7075-T6 bulk material (plain view). Irregular shaped intermetallic particles can be seen clearly aligned along lines in the rolling direction. Figure 2b shows microstructure of the 7075 sample sintered at 500 $^{\circ}\text{C}$. After sintered at 500 $^{\circ}\text{C}$ for 15 min, a sintered compact with a relative density of 98.6% was obtained, only limited number of pores can be observed. In contrast to the bulk sample, very few intermetallic particles can be seen sparsely distributed in the sintered sample. It indicated that as a result of rapid solidification, most of the solute atoms are remained dissolved in the alloy matrix or the intermetallic particles are too small to be detected.

Figure 3 shows the effect of sintering temperature on the grain size of the sintered samples. Grain growth is obvious and the growth rate increased sharply when the sintering temperature is higher than 500 $^{\circ}\text{C}$. Thus, 500 $^{\circ}\text{C}$ was chosen to be the optimal sintering temperature in this study and the resulting grain size is about 17 μm , which is quite small when compared to that of the bulk alloy (about 82 μm). The measured density and hardness of the sample sintered at 500 $^{\circ}\text{C}$ are listed in Table 1.

Figure 4 depicts potentiodynamic polarization scans of the bulk and sintered 7075 samples in 0.1 M NaCl solution, the potential E in V versus a saturated

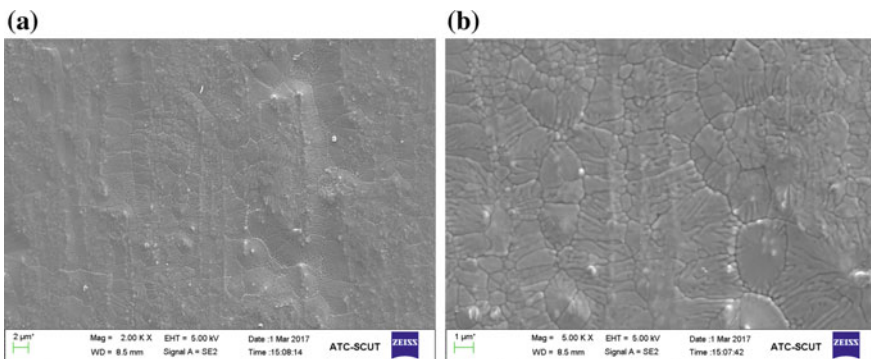


Fig. 1 SEM micrographs of melt-spun 7075 ribbon (free-side) (b) is the enlarged image of (a)

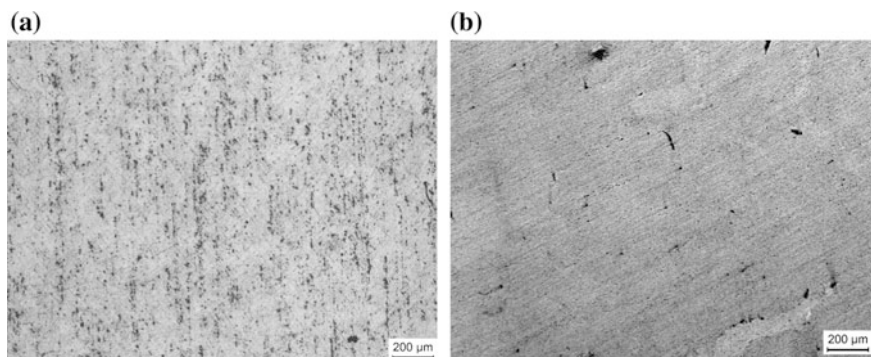


Fig. 2 Optical micrographs of **a** 7075-T6 bulk and **b** sintered 7075 samples

Fig. 3 Effect of sintering temperature on the grain size of the sintered samples

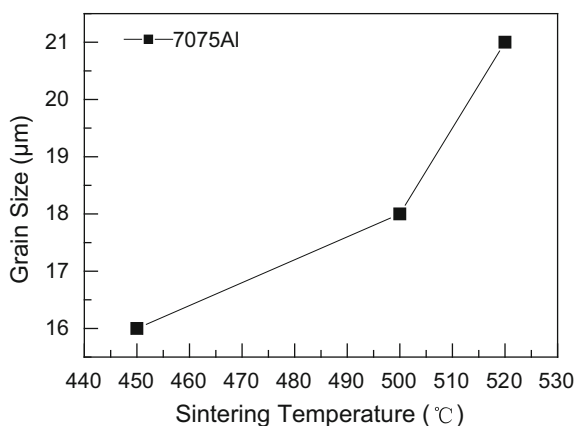
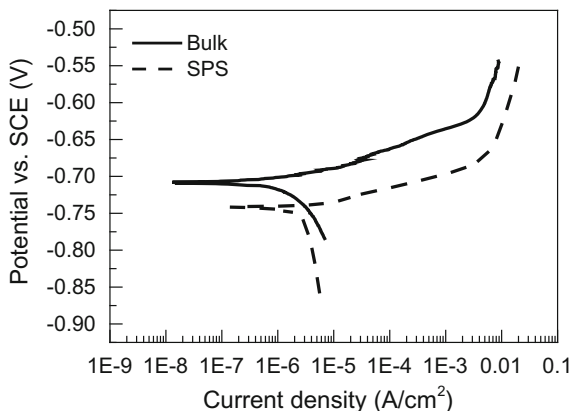


Table 1 Hardness, density and electrochemical test results (in 0.1 M NaCl) of the samples

Sample	Hardness (HV)	Density (g/cm ³)	E _{corr} (V)	OCP (V)	I _{corr} × 10 ⁻⁶ A cm ⁻²
7075-T6 Bulk	171.3 ± 3.8	2.81	-0.71 ± 0.03	-0.73 ± 0.02	3.52 ± 1.85
7075 Sintered	84.6 ± 2.2	2.77 ± 0.13	-0.74 ± 0.01	-	6.09 ± 2.15

calomel electrode (SCE) as a function of current density (*i*) was shown. The electrochemical corrosion experiment results are summarized in Table 1. As demonstrated in Table 1 and Fig. 4, when immersed in 0.1 M NaCl solution, the sintered sample showed a drop of 0.03 V (versus SCE) compared to the E_{corr} of the bulk sample. That means the tendency of the sintered alloy to corrode is a little bit

Fig. 4 Potentiodynamic polarization scans of the bulk and sintered samples in 0.1 M NaCl solution



higher. Similar trend can be observed in the corrosion rate (I_{corr} , current at corrosion potential). The lower corrosion resistant of the sintered 7075 alloy is because of the existence of porosity, since NaCl solution can penetrate into the surface pores and corroded the sub-surface grains just below the sintered alloy surface. Although the porosity is not high at all in the studied sample, the exposed pores did affect adversely on the corrosion behavior of the sintered sample. However, it is believed that the significance of the quality of inter-particle bonding is the dominant factor in this case, since Al alloys are hard to be sintered because of the protective surface oxide. As pointed out by Spencer and Zhang: “Coating with better inter-particle bonding will be less subjected to localized attack.” [13]. From Fig. 2, it is obvious that the quality of inter-particle bonding in the sintered sample is not comparable to those of the bulk sample.

Figure 5 shows optical micrographs of the bulk and sintered samples after immersion in 0.1 and 0.6 M NaCl solution for 7 days. For comparison, the area ratios of the corrosion characteristic in different samples are listed in Table 2. Pits and pores both appeared as dark areas in the micrographs, so they cannot be distinguished by image analyzer. The cathodic protection zones (CPZ) are white areas around the pits. Many corrosion craters with different sizes can be seen in the bulk samples after immersion tests, especially for those immersed in 0.6 M NaCl solution.

By careful inspection, these craters are quite shallow and bumpy at the bottom. These craters are believed to be originated from the pitting of anodic zones that located at or in the vicinity of grain boundaries and caused intergranular corrosion (IGC). The progressing IGC eventually leads to the falling out of the surface material and leading to craters. Large irregular shaped corrosion craters that found in the bulk samples are absence, but typical feature of pit corrosion that surrounded by cathodic protecting zone can be seen in the sintered samples. The localized pitting attack is usually associated with the embedded particles in the matrix that exposed to the open surface. Pits may either initiate at the matrix near noble particles, which are cathodic to the matrix, or at active particles, which are anodic to

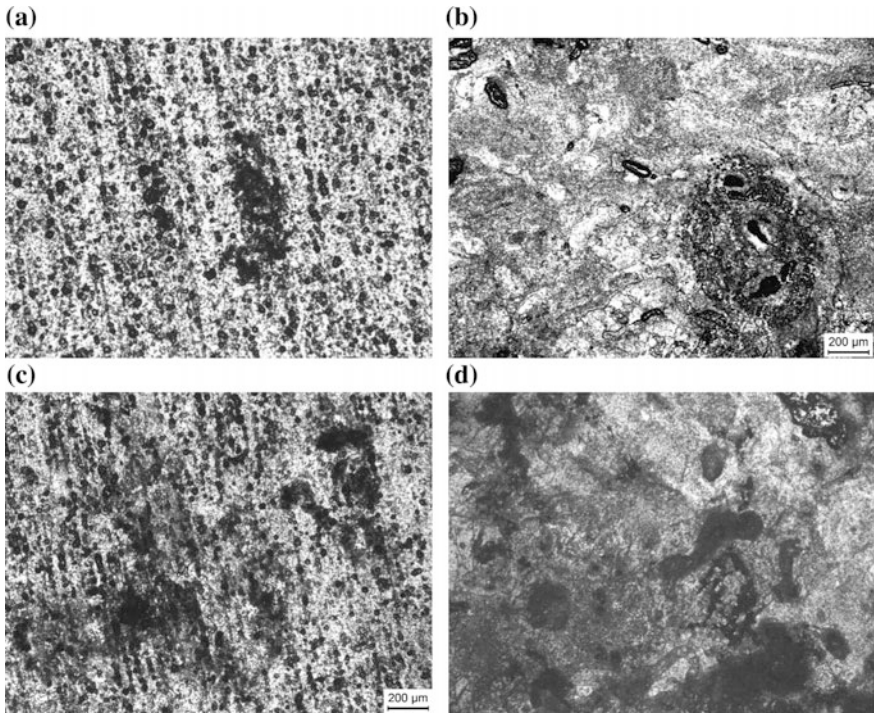


Fig. 5 Micrographs of the bulk (a, c at left) and sintered (b, d at right) 7075 samples after immersion in 0.1 M (top row) and 0.6 M (bottom row) NaCl solution for 7 days. All images share the scale bar

Table 2 Average area ratios of the corrosion characteristic after immersing the bulk and sintered samples in NaCl solution

Sample	Pit/Pores	CPZ	GC	Pit/Pores	CPZ	GC
7075-T6 Bulk	0.12 ± 0.03	–	–	0.19 ± 0.01	–	–
7075 Sintered	0.07 ± 0.03	0.13 ± 0.06	0.80 ± 0.06	0.09 ± 0.03	0.21 ± 0.06	0.70 ± 0.06

Note For bulk sample the balance resembles not corroded surface

the matrix, and thereby preferentially corroded. The pitting corrosion that found in sintered samples belongs to the later type. Due to the fine grain microstructure of the sintered sample, the number density of pits is high and the average size of the pits is small. Besides, the surface voids in the sintered sample increased the contacting surfaces between the alloy and the NaCl solution, which leads to much more pit initiating sites, so general corrosion (GC) is the major corrosion phenomena in the sintered samples. From Table 2, by comparing the quantified corrosion characteristics, such as pit/pores, CPZ and GC, of the sintered samples after immersed

in 0.1 and 0.6 M NaCl solution, no big different can be observed, therefore, it can be concluded that not much decrease in corrosion resistance when the sintered 7075 alloy exposed to a harsher environment (0.6 M NaCl solution) as compared to milder corrosion condition (0.1 M NaCl solution).

Conclusions

Rapidly solidified 7075 Al alloy ribbon obtained by melt-spinning were sintered into compacts with a relative density of 98.6% by spark plasma sintering at the optimal sintering temperature of 500 °C. Results on Corrosion behavior of the 7075 bulk and sintered materials indicated that porosity adversely affected the corrosion behavior of the material in NaCl solution. The sintered material exhibited slightly lower corrosion resistance than the bulk 7075 alloy. Immersion experiment results showed that even in a harsher environment (0.6 M NaCl solution), there is not much decrease in corrosion resistance of the sintered 7075 as compared to the bulk material.

References

1. E.J. Lavernia, J.D. Ayers, T. Srivatsan, Rapid solidification processing with specific application to aluminum alloys, *Int. Mater. Rev.* 37 (1992) 1–44.
2. C.L. Xu, H.Y. Wang, F. Qiu, Y.F. Yang, Q.C. Jiang, Cooling rate and microstructure of rapidly solidified Al-20wt.% Si alloy, *Mater. Sci. Eng. A* 417 (2006) 275–280.
3. Y. Birol, Microstructural evolution during annealing of a rapidly solidified Al-12Si alloy, *J. Alloys. Compd.* 439 (2007) 81–86.
4. A.K. Srivastava, V.C. Srivastava, A. Gloter, S.N. Ojha, Microstructural features induced by spray processing and hot extrusion of an Al-18% Si-5% Fe-1.5% Cu alloy, *Acta. Mater.* 54 (2006) 1741–1748.
5. Y.E. Kalay, L.S. Chumbley, I.E. Anderson, R.E. Napolitano, Characterization of hypereutectic Al-Si powders solidified under far-from equilibrium conditions, *Metall. Mater. Trans. A* 38 (2007) 1452–1457.
6. T. Hu, K. Ma, T.D. Topping, J.M. Schoenung, E.J. Lavernia, Precipitation phenomena in an ultrafine-grained Al alloy, *Acta Mater.* 61 (2013) 2163–2178.
7. V.K. Champagne, The repair of magnesium rotorcraft components by cold spray, *J. Fail. Anal. Prev.* 8 (2008) 164–175.
8. K.K. Sankaran, R. Perez, K.V. Jata, Effects of pitting corrosion on the fatigue behavior of aluminum alloy 7075-T6: modeling and experimental studies, *Mater. Sci. Eng. A* 297 (2001) 223–229.
9. P.S. Pao, S.J. Gill, C.R. Feng, On fatigue crack initiation from corrosion pits in 7075-T7351 aluminum alloy, *Scr. Mater.* 43 (2000) 391–396.
10. M.R. Rokni, C.A. Widener, G.A. Crawford, Microstructural evolution of 7075 Al gas atomized powder and high-pressure cold sprayed deposition, *Surf. Coatings Technol.* 251 (2014) 254–263.
11. Y. Qu, R. Su, J. You, R. Li, Study on microstructure, mechanical properties and corrosion behavior of spray formed 7075 alloy, *Mater. Today Com.* 4 (2015) 109–115.

12. V.V. Rao, Centrifugal atomization and rapid-solidification processing of high-strength aluminium alloys, *J. Mater. Sci. Let.* 11 (1992) 135–137.
13. K. Spencer, M.X. Zhang, Optimization of stainless steel cold spray coatings using mixed particle size distributions, *Surf. Coatings Technol.* 205 (2011) 5135–5140.